International Journal of Mechanical, Industrial and Aerospace Sciences
ISSN: 2517-9950
Vol:7, No:4, 2013

# Dominant Flow Features of Two Inclined Impinging Jets Confined in Large Enclosure

T. Chammem, H. Mhiri, and O. Vauquelin

***Abstract*****—**The present study was provided to examine the vortical structures generated by two inclined impinging jets with experimental and numerical investigations. The jets are issuing with a pitch angle α=40° into a confined quiescent fluid. The experimental investigation on flow patterns was visualized by using olive particles injected into the jets illuminated by Nd:Yag laser light to reveal the finer details of the confined jets interaction. It was observed that two counter-rotating vortex pairs (CVPs) were generated in the near region. A numerical investigation was also performed. First, the numerical results were validates against the experimental results and then the numerical model was used to study the effect of section ratio on the evolution of the CVPs. Our results show promising agreement with experimental data, and indicate that our model has the potential to produce useful and accurate data regarding the evolution of CVPs.

***Keywords*****—**Inclined impinging jets, counter-rotating vortex pair, CFD, experimental investigation, section ratio.

## I. Introduction

MANY experimental and numerical studies have been devoted to the investigation of the behavior of simple jet issuing into a crossflow [1]. In general four main coherent structures [2] characterize the jet in crossflow: (i) the counter-rotating vortex pair (CVP), which originates in the near field of the jet and essentially follows the jet trajectory and dominates the flow field far downstream; (ii) the shear-layer vortices which are located at the upstream side of the jet and take the form of ring-like or loop-like filaments; (iii) horseshoe vortices forming in the flat-plate boundary layer upstream of the jet exit and corresponding wall vortices downstream of the exit close to the wall; and (iv) 'wake vortices/upright vortices' which are vertically oriented shedding vortices in the wake of the jet. Yuan et al [3] have identified other structures named the hanging vortices. The hanging vortices are found near the jet exit.

The CVP still the most dominant vortical structures [2], [4], [5], [6], [7]. They confirm that all deflected jets must contain a pair of counter-rotating vortices. There are relatively less studies on multiple jets issuing into a crossflow where the flow represents an interaction of two or more jet in crossflow [8], [9], [10]. In their studies they investigate the global characteristics of multiple jets field by varying the number or the geometrical configuration of jets. V. Kolar et al [11]-[13] studied the effect of three nozzle arrangements on the evolution of the dominant vertical mean flow structures. They found that for geometrically symmetric arrangements (tandem ad side-by-side) the mean flow becomes rapidly similar to that of single jet in crossflow. For an oblique ground arrangement, the resulting CVP exhibits a nature asymmetry. But it resembles the structures of the single jet. The counter-rotating vortex is, only, much stronger than that of the single jet. For the three arrangements, the deflected jets are dominant by one single resulting counter-rotating pair, instead of two pairs. In opposed jet configuration, R.L.J.Fernandes et al [l4] shows, in his study on the interaction of two opposed round jets issuing into a small aspect ratio channel cross flow, that the interaction of jets at a high momentum flux ratio (J=155) generates a pair of vortices upstream of the impingement region. Perchanok et al [15] indicate the formation of two pairs of recirculation zones; one pair upstream and one pair downstream of the jets. Chen and Hwang [16] argue the development of a pair of recirculation zones at the cross-flow walls immediately downstream of each of the jet exits. In inclined impinging jets configuration, Kazuyoshi Nakabe et al [17] investigate the interaction between two impinging jets in in-line and staggered arrangement with cross flow. They found four aligned longitudinal vortices in the case of staggered arrangement of the two inclined jets, but they observe only three major vortices in the case of in-line arrangement.

In spite of their large applications, confined impinging jets have received very little attention. In this study, dominate structures generated by two inclined jets issuing into a big channel (without crossflow initially) are experimentally studied by using tomography laser for visualizations and numerically investigated by means of a finite volume code using the commercially CFD software Fluent 12.1.4. Four turbulent models have been tested; three first order models; the standard k-ε model, the RNG k-ε model and the realizable k-ε and a second-order model RSM model. In this case the crossflow is generated by inducing longitudinal flow depending on the entrainment of surrounding fluid into jets. In fact, the idea in this work consists in injecting external air with two inclined jets to induce longitudinal air flow in large enclosure.

The flow pattern in both the interaction region and the near region of resulting jet is very complex. This paper was undertaken to bring useful experimental and numerical information predominantly on dominant features on two inclined impinging jets issuing into confined duct. First, the experimental technique and the numerical models were described. The numerical results were, then, compared to the experimental visualization. Finally, numerical investigations

T. Chammem is with the IUSTI, Technopôle de Château-Gombert, 5 rue Enrico Fermi, 13 013 Marseille, France and the UTTPI, Ecole Nationale d'Ingénieurs de Monastir, Route de Ouardanine, 5000 Monastir, Tunisia
(Phone: 0021622577221; e-mail: chamem_tebr@yahoo.fr).
H. Mhiri, is with the UTTPI, Ecole Nationale d'Ingénieurs de Monastir, Route de Ouardanine, 5000 Monastir, Tunisia
O. Vauquelin is with the IUSTI, Technopôle de Château-Gombert, 5 rue Enrico Fermi, 13 013 Marseille, France.

were presented to describe the vertical structures evolution with various surface ratios SR (defined as the ratio of the tunnel section to the jet section) as in detail.

## II. Experimental Set-up and Numerical Methods

### A. Experimental Set-up

An overall view of the experimental setup is shown in Fig.1. The equipment consists of a scaled model representing a prototype tunnel with rectangular cross-section, measuring L x W x H = 100 x 6 x 8 $m^3$. Two lateral inclined jets with 0.6 m hydraulic diameter impinge in the middle of the tunnel. The jet outlet velocity was held constant at $V_j$=10m/s. The jets discharge at a pitch angle α=40°. The pitch angle α is the angle between the direction normal to the wall and the jet centerline. The duct length upstream of the discharge nozzle was 1m to ensure a fully developed velocity profile at the exit. A honeycomb installed at the PVC duct assists the smoothing and alignment of the flow breaking large scale eddies to smaller ones. The scale model was constructed by Plexiglas to accommodate airflow visualization.

Visualization of the air flow generated by two inclined and impinging jets was done in the near region and downstream jets interaction. Both air jets are sowed by fine olive oil particles (~3-4μm in diameter) and lightened by Nd:YAG Laser of 532nm wavelength. The seeding system is an atomizer based on Venturi principle to produce fine particles. It allows distribution of particles with more or less homogeneous sizes and in sufficient amount. The seeding for the jets is introduced into the manifold to effect equal seeding between the jets.

A CCD camera with spatial resolution of 1280x1024 pixels is placed in front of the laser light plane to obtain visual pictures of velocity field. The experiments were carried out on airflow without any external stream. The two jets consist of air at ambient temperature for which the dynamic viscosity μ = 1.78 x $10^{-5}$ kg/m.s, and the density ρ=1.22 kg/$m^3$. Under these conditions, the flow may be considered to be Newtonian, incompressible and isotherm.

### B. Numerical Methods

Only experimental results make it difficult to investigate the entire configurations for parametric study. For this reason, numerical investigation was performed to provide more detailed picture of the vertical structures.

The physical domain under investigation is shown in Fig. 2. The tunnel concerned was simplified as a rectangular tube. The jets were confined in a large enclosure. The pitch angle was fixed at 40° for both jets. The injection Reynolds number based on the hydraulic diameter of both jet, $Re_j$, was fixed to be constant; Rej = $U_j d/\nu \approx 4 \times 10^5$ (where $U_j$ is the jet exit velocity, d is the hydraulic diameter of the nozzle and ν is the kinematics viscosity).

Three-dimensional geometry is divided in two types of zone; A and B. The zone A is the domain around the two jets that is created with unstructured tetrahedral meshing scheme. However, zone B is the remaining volume that is created with structured hexahedral meshing scheme. A 0.2 m mesh for zone A and a 0.4 m mesh for zone B were chosen. The mesh dimensions were chosen in a way the trade-off between the accuracy of numerical results and the computational time is reached. Velocity inlet boundary condition is used at the nozzles inlet. Pressure outlet boundary condition is used for the tunnel outlet. Pressure inlet boundary condition is used for the tunnel inlet. The wall boundary condition is enforced at the tunnel walls.

Simulations were conducted using the commercially CFD software Fluent 12.1.4 based on the finite volume approach to solve the conservation laws of mass and momentum. The flow was assumed to be three-dimensional, steady-state, incompressible and turbulent. The velocity and pressure terms of momentum equations are solved by the SIMPLE method.

## III. Results and Discussion

### A. Models of Turbulence Dependence

Four different turbulence models (three high-Re models with wall function; standard k-ε, RNG k-ε, realizable k-ε

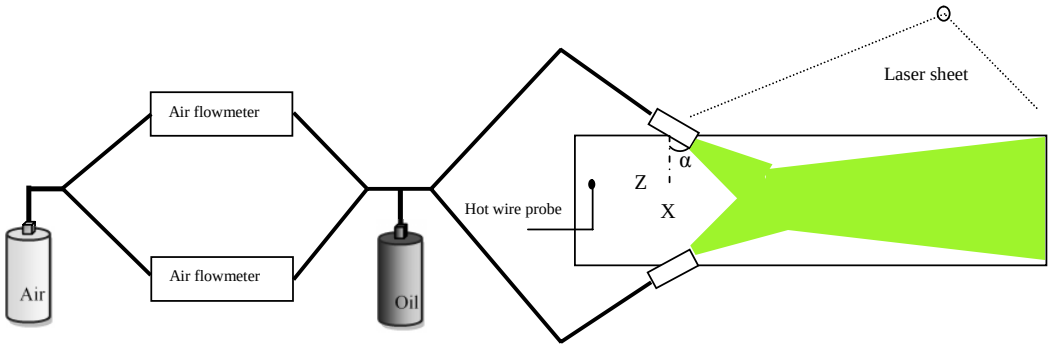


Fig. 1 Sketch of the experimental set-up

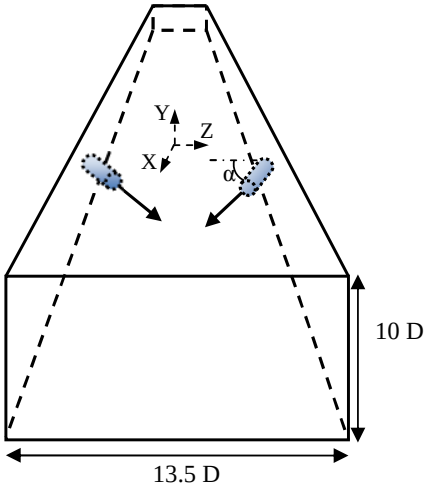


Fig. 2 schematic diagram showing the computational domain, the jets pitch angle fixed at 40°

and a low-Re model; RSM) were used for the prediction of the mean velocity and the turbulent intensity in the near region. Figs. 3 and 4 compare the mean velocity profiles and the turbulence intensity at a fixed x/d=1 and SR=48 for various turbulence models, respectively. Results show that the mean velocity profiles agreed well using different models, whereas there were some discrepancies in the turbulent intensity profiles for the RNG k-ε model.

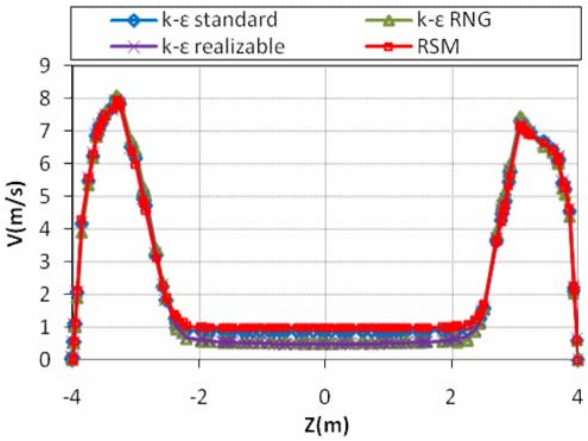


Fig. 3 Mean velocity evolution at X/D = 1 from the nozzles exit

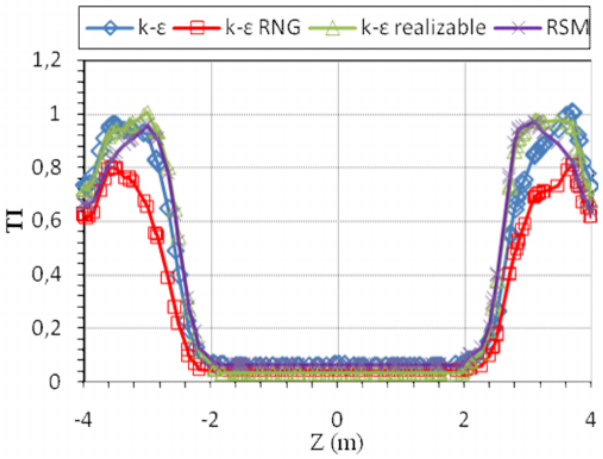


Fig. 4 Turbulence intensity evolution (TI) at X/D = 1 from the nozzles exit

The standard k-ε model was chosen as turbulence model for the further evaluations. In the literature, some researches [18, 19] indicated that the *k– ε* model of turbulence was the most appropriate model for practical building airflow applications and still the least time consuming approach. However, due to its simplicity, its accuracy is limited, particularly when analyzing complex, three-dimensional flow in buildings [20,

21]. The main weakness of the traditional $k-\varepsilon$ model is its failure to model near-laminar (low-Reynolds-number) flow [22]. This degrades accuracy, especially when modeling large space buildings with pronounced wall effect. To account for it, a near-wall model approach called the «enhanced wall treatment» has been used in the vicinity of the wall [23, 24]. In this approach the viscosity affected near-wall region is completely resolved along the way to the viscous sublayer. Generally, it requires a very fine near-wall mesh, see Fig. 5. The first grid point off the wall must be from $y^+<3$. Furthermore a refinement of the mesh for the low Reynolds number in the near wall region is necessary.

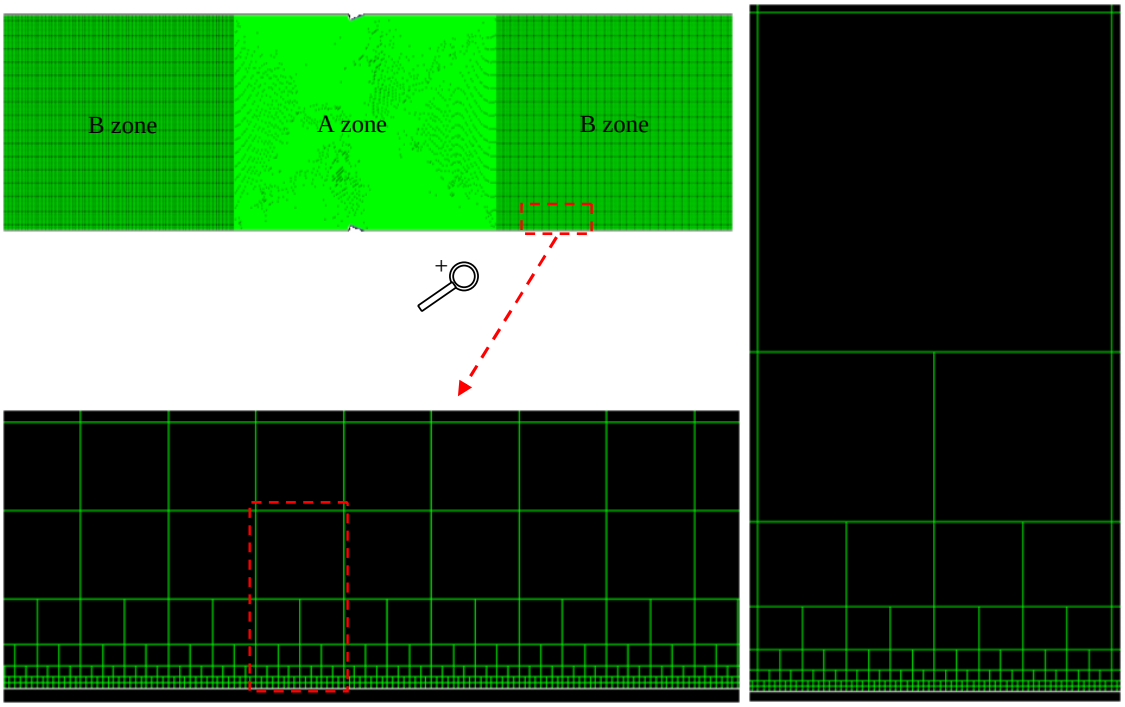


Fig. 5 Computational grid at some of the domain surfaces showing mesh in the sublayer zone

*B. Dominant Vertical Structures*

Flow visualizations studies have revealed the existence of several vertical structures, and have indicated the importance of their dynamics. The CVPs are reported to be the most dominant structures persisting far downstream of the jets nozzles. The CVPs can, only, be visualized when particles were seeded in the surrounding fluid and not when seeded in the jets. Fig. 6 is a visualization of streamwise and cross-stream, showing (in the left) the jets impingement and the resulting jet formation and the CVPs generation (in the right) at one downstream location x/d=10. The visualization demonstrates the generation of four vortices forming two CVPs.

To illustrate the formation of vertical structures, we examine two flow quantities, pressure and velocity; they are plotted as streamlines and vectors in Figs. 7 and 8, respectively. Pressure streamlines mark the locations of the low-pressure cores of vertical structures in the flow field.

Fig. 7 shows the streamlines and pressure distribution in various transversal plans of the two impinging confined jets.

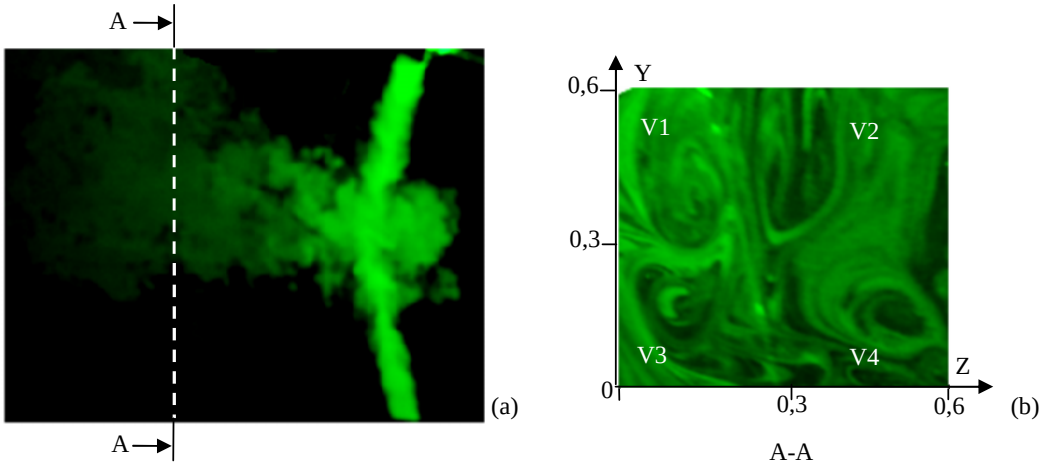


Fig. 6 Instantaneous images of the impinging jets: (a) Streamwise plane showing the twin inclined jets and the resulting jet, (b) Visualization of counter-rotating vortices in cross-stream plane at one downstream location x/d=10 from the jet exit nozzle

There were four low-pressure zones on the vortices center. These low-pressure zones extended into the domain up to a certain distance downstream the jet and then gradually increased to reach atmospheric pressure. As a result, the counter-rotating vortices occurred in the cross section. The pressure difference provides the force that deforms the jet and contributes to the development of the CVPs prominent structures.

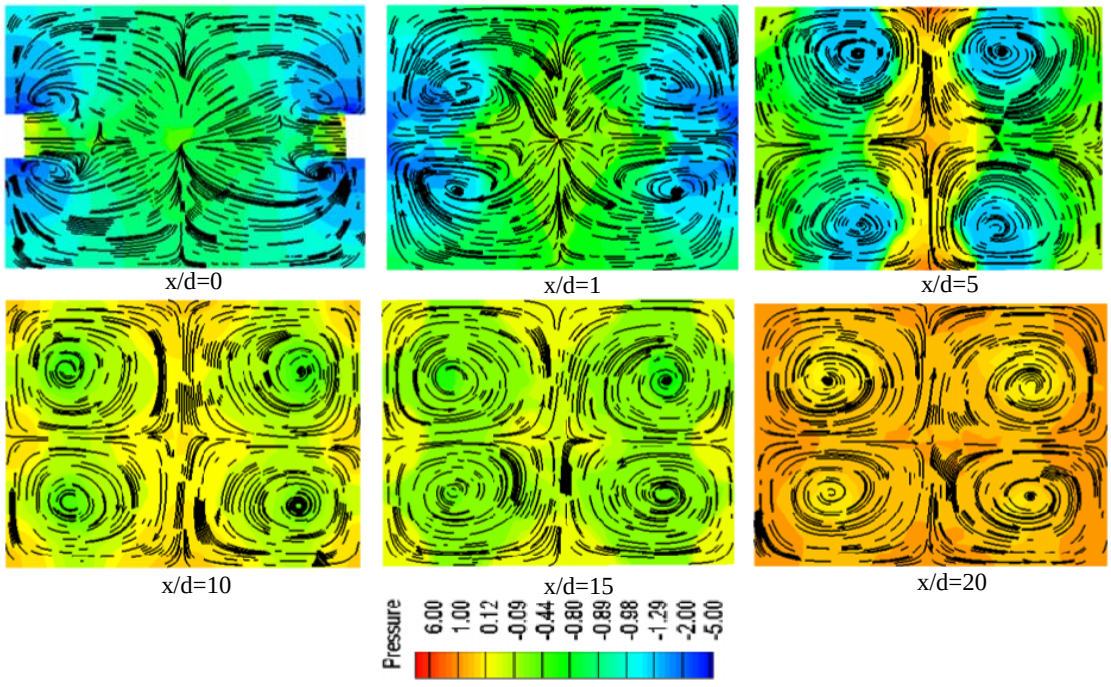


Fig. 7 cross-stream pressures streamline plots at six downstream locations, showing the initiation and formation of streamwise vortices

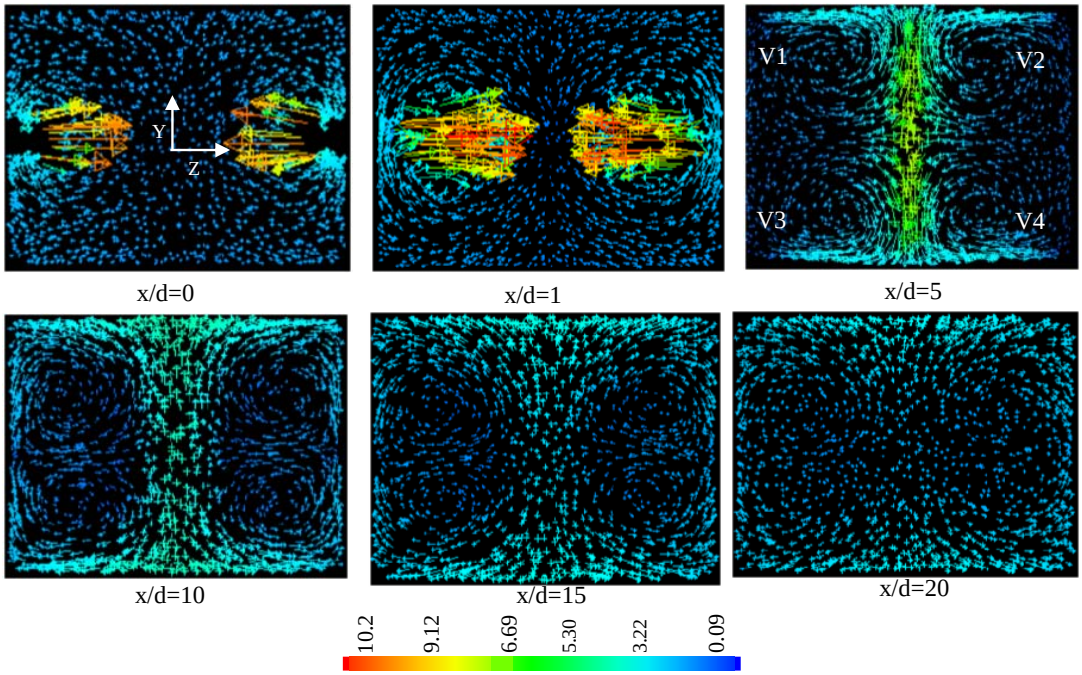


Fig. 8 Evolution of the counter-rotating vortex pairs generated by tow inclined impinging jets confined in large enclosure at x/d=0, x/d=1, x/d=5, x/d=10, x/d=15et x/d=20, Re=4x10$^5$ and α=40°

Fig. 8 is a vector plot of the mean velocities at selected axial positions. It shows the existence of four identical transversal vortices generated by the two inclined impinging jets at six streamwise locations in the near region, x/d<20; x/d=0, x/d=1, x/d=5, x/d=10, x/d=15 and x/d=20. The vector plot identifies the formation of the hanging vortices as a strong vortex at the side of each jet. These vortices are related to the skewed mixing layer on the sides of the jets. The core of each jet is composed of two large-scale counter-rotating vortices on which shear-layer instabilities develop.

It can be seen that the vortices forming each of the pairs are rotating in opposite directions. The vortices V2 and V3 with clockwise rotation and vortices V1 and V4 with anti-clockwise rotation were observed in the cross-sections downstream jets. The rotational sense of the streamwise vortices is outwardly spreading. The counter-rotating rotational sense of the streamwise vortices also meant that the ambient fluid will be entrained into the jet body. Therefore, the formation and persistent presence of the stream vortices aid mixing between the jets and their surroundings by promoting greater levels of momentum exchange.

As the jet flows convect downstream, the vortex-core sizes of the streamwise vortices increase gradually occupying almost the whole cross-section of the jet. They also gradually become more unsteady with increase in downstream distance (in addition to their relatively weak strengths owing to diffusion of vorticity) and yet remain essentially unmixed. We can see also that the confining walls limit the growth of the counter-rotating vortices.

The pairs grow up along the streamwise direction, but far downstream the four vortices disappear (x/d=20). We can conclude that these vortices have a finite span during which they translate in the axial direction with a range of motion of about 20 diameters.

Experimental visualization is used to examine this configuration further. The visualized cross section, which is a photograph at x/d=10, shows two pairs of counter-rotating vortices were generated downstream of the two jets.

### *C. Dynamics of CVPs for Impinging Jets*

1. Peaks Location

Figs. 9 and 10 provide a summary of the downstream location of the V2 peak (where the vorticity is maximum). The z-locations and the y-locations of CVPs peaks are depicted.

Figs. 9 and 10 show that the z-locations and the y-locations of vorticity peaks decrease with surface ratios.

It is found that the peak z-position convicts, first, towards the wall and then changes direction to regain the centre, see Fig. 9. Comparison between the z-locations for various RS shows that the vortex moves away from the centre as the RS increases.

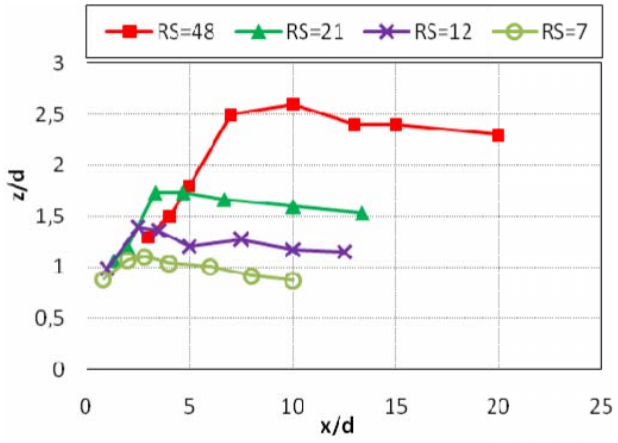


Fig. 9 Downstream locations of counter-rotating vortex pairs V2 for different surface ratios

In the first stage the peaks moves toward the walls because of the Coanda effect. In fact, the entrainment of the jets is disturbed by the wall and, due the impossibility to entrain the wall, the jets move toward the walls and the distance between the vortices centers increase. Further downstream, the vortices growth and spread. The entrainment is, here, disturbed and the jets bend towards other one as each jet try to entrain the other. The peaks location move a little towards the centre.

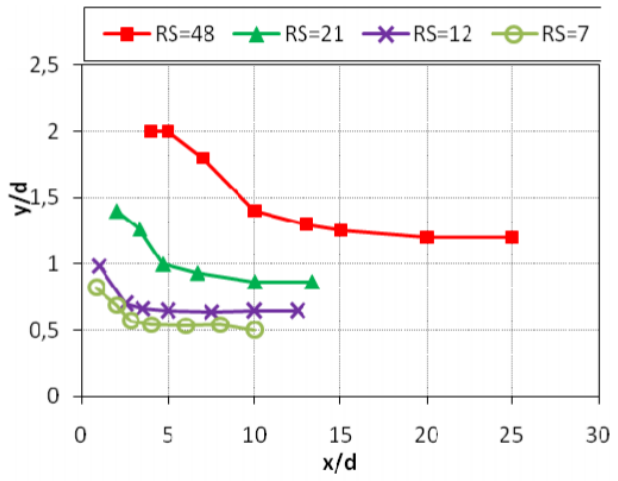


Fig. 10 Comparison of V2 peaks y-location between different surface ratios

The y-locations decrease and then still situated at the same position around y/d= 1.2 for a RS=48, y/d=0.9 for RS=21, y/d=0.6 for RS=12 and around y/d=0.5 for RS=7. The position of the rotating vortex moves away from the tunnel centre in y-direction as the RS increased. This behavior is due to the fact that, at lower RS the CVPs are stronger and tend to merge together quickly. Whereas, when the RS is high the CVP tend, initially, to bend towards the wall near the jets exit. It is concluded that, as the distance from the jets exit increases, the y-position of the CVPs center decreases at all section ratios. The spanwise distance between the CVPs centers decrease as the distance from the jet exit increases.

*2.* Vorticity Transport

The vorticity transport analysis shows the vortex-strength decay. The turbulent vorticity transport is driven by the gradients of Reynolds stress tensor components and anisotropy and inhomogeneity of Reynolds stresses.

By transforming the momentum equation

$$\frac{\partial u}{\partial t} + (u.\Delta)u = -\frac{1}{\rho}\nabla p + \nu \nabla^2 u \quad (1)$$

into an equation for the vorticity $\omega = \nabla \times u$ the vorticity transport equation for incompressible flows is given by:

$$\frac{D\omega}{Dt} = \omega.\nabla u + \nu \nabla^2 \omega \quad (2)$$

where (ω) is the distribution of vorticity and (u) is the velocity field.

The vorticity transport equation shows that the rate of change of the vorticity $D\omega/Dt$, is controlled by 'vortex stretching' (described by $(\omega \cdot \nabla u)$) and by diffusion (described by $\nu \nabla^2 \omega$).

This transport is supposed to be the main cause of the cancellation of the vortex strength of the CVPs in terms of circulation. We represent in the following paragraph the evolution of the vorticity downstream jets.

Fig. 11 shows the total vorticity evolution for different sections ratios (RS). The downstream development of the vorticity is clearly dependent on the section ratios. By comparing the counter-rotating vortex pairs in terms of vorticity, the smaller sections ratio exhibits the much higher turbulent vorticity, in the near region, and the much stronger vortex strength (Fig.12). The counter-rotating vortex pairs disappear faster for the smaller section ratio.

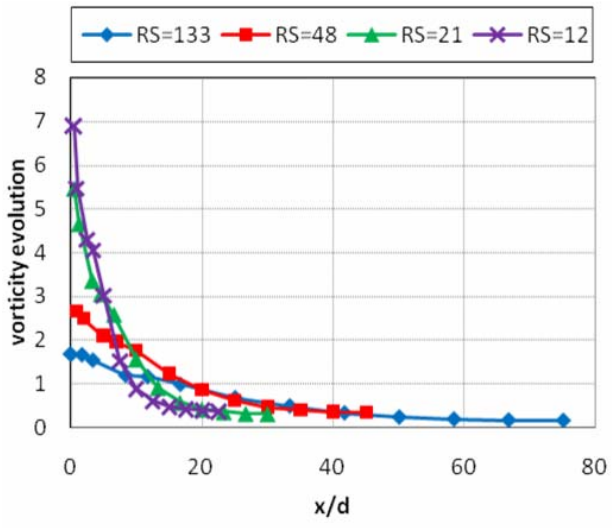


Fig. 11 Total vorticity evolution

The formation of two CVPs was more prominent for smaller RS in the near region. For RS=12 those vortex pairs extended to x/d=20, for RS=21 the vortex pairs extended to x/d=25, for RS=48 the vortex pairs extended to x/d=40 and for RS=133 the vortex pairs extended further, to x/d=60. The lower section ratio results in a more pronounced vorticity distribution of the height of the peak vorticity with the smaller distance extent downstream

## IV. Conclusion

The present study is an investigation of the dominant flow features of two inclined jets confined into large enclosure. This work concentrates upon the vorticity distribution and the counter-rotating vortex pairs which dominate the flow behavior.

Experimental and numerical results obtained in the present study are summarized as follows:

1. It is shown, unlike, to the last studies the existence of two counter-rotating vortex pairs which are responsible for the entrainment of the surrounding flow.

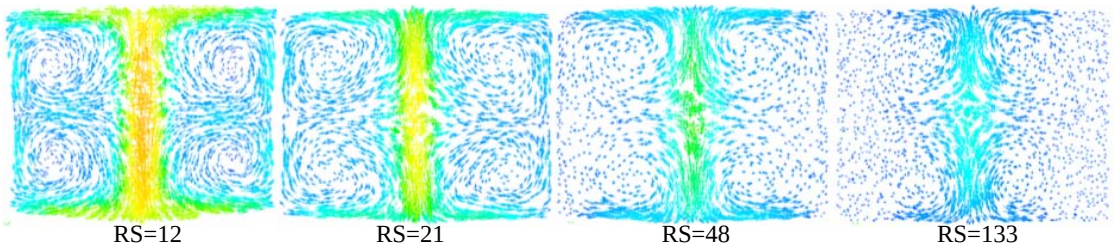


Fig. 12 For various surface ratios at x = 5

2. The CVPs evolves downstream in the longitudinal direction X and its strength decreases.
3. The vortical structures are more complex than for a single jet. It was found that the interaction between the two jets has significant effect on the formation of transversal vortices.
4. The impingement of two inclined jets results in one simple jet downstream the interaction point. However, they are two counter-rotating vortex pairs unlike the simple jet. The two counter-rotating vortex pairs are generated in the rectangular large enclosure as the result of inclined impinging jets.
5. As the distance from the jet exit increases, the y-position of the CVPs centers decreases and the distance between the CVPs centers decreases.
6. As the jet distance from the jet exit increases, the z-position of the CVPs center increases and then decreases.
7. The effect of the section ratios on the evolution of the counter-rotating vortex has been investigated in this paper. The CVPs get stronger, as the section ratio decreases in the near region and dissipated faster.
8. The present k-ε computations have proven the ability of reproducing the dominant features of impinging jets issuing into a confined large enclosure.

## References

[1] R.J. Margason, "Fifty years of jet in cross flow research. In Computational and Experimental Assessment of Jets in Cross Flow. Proceedings of NATO AGARD Conference, CP-534, Winchester, UK. 1993.
[2] T.F. Fric, A. Roshko, "Vortical structure in the wake of a transverse jet," Journal of Fluid Mechanics, vol. 279, pp. 1–47, 1993.
[3] L. L.Yuan, R. L. Street, & J. H. Ferziger, "Large-eddy simulations of a round jet in crossflow," J. Fluid Mech. Vol. 379, pp.71–104, 1999.
[4] B.R. Morton, A. Ibbetson, "Jets deflected in a crossflow," Experimental Thermal and Fluid Science, vol. 12, pp.112–133, 1996.
[5] J. F. Keffer and W. D. Bains, "The Round turbulent jet in a cross-wind," J. Fluid Mech. Vol. 15, pp. 481-496, 1963.
[6] K.B. Mc Grattan. H.R. Baum and R.G. Rehm," Numerical simulation of smoke plumes from large oil fires," Atmospheric Environment, vol. 30, pp. 4125-4136, 1996.
[7] R. Fearn, and R.P. Weston, "Vorticity associated with a jet in a crossflow," AIAA J. vol. 12, pp. 1671-1975, 1666.
[8] M. Gregoric, L.R. Davis, D.J. Bushnell, "An experimental investigation of merging buoyant jets in a crossflow." ASME J. Heat Transfer, vol. 104, pp. 236–240, 1982.
[9] A.R. Karagozian, T.T. Nguyen, C.N. Kim, "Vortex modeling of single and multiple dilution jet mixing in a cross flow," J. Propul. Power 2, 354–360, 1986.

[10] J.M.M. Barata, D.F.G. Durao, M.V. Heitor, J.J. McGuirk, "Impingement of single and twin turbulent jets through a crossflow," AIAA J. vol.29, pp.595–602, 1991.
[11] V. Kolar, H. Takao, T. Todoroki, E. Savory, S. Okamoto, N. Toy, "Vorticity transport within twin jets in crossflow," Exp. Therm. Fluid Sci. vol.27, pp.563–571, 2003.
[12] V. Kolar, E. Savory, H. Takao, T. Todoroki, S. Okamoto, N. Toy, "Vorticity and circulation aspects of twin jets in crossflow for an oblique nozzle arrangement," IMechE J. Aerospace Eng. Vol.220, pp.247–252, 2006.
[13] V.Kolar, E. Savory, "Dominant flow features of twin jets and plumes in crossflow," Journal of Wind Engineering and Industrial Aerodynamics vol."95, pp.1199–1215, 2007.
[14] R.L.J.Fernandes., A. Sobiesiak., A. Pollard., opposit round jets issuing into a small aspect ratio channel cross flow," Experimental Thermal and Fluid Science. Vol.13, pp.374-394, 1996.
[15] M. S. Perchanok, D. M. Bruce, I. S. Gartshore, "Velocity measurements in an isothermal scale model of a hog fuel boiler furnace," J, Pulp Paper Sci. vol.15, pp.212-219, 1989.
[16] K. S. Chen, J,Y. Hwang, "Experimental study on the mixing of one and Dual-Line heated jets with a cold crossflow in a confined channel," AIAA J, vol.29, pp.353-360, 1991.
[17] Kazuyoshi Nakabe, Elzbieta Fornalik, Jens F. Eschenbacher et al., "Ineractions of longitudinal vortices generated by twin inclined jets and enhancement of impingement heat transfer," International Journal of heat and fluid flow,vol.22, pp.287-292, 2001.
[18] EH. Mathews, "Numerical solutions of fluid problems related to buildings, structures and the environment," Building and Environment, 24 (1):1. 1989.
[19] BE. Launder, DB. Spalding, "The numerical computation of turbulent flows," Computer Methods in Applied Mechanics and Engineering, vol.3, pp.269–89, 1974.
[20] S. Murakami, "Prediction, analysis and design for indoor climate in large enclosures," Roomvent '92. In: Proceedings of third international conference. DANVAK, 1992.
[21] Q. Chen, Z. Jiang, "Significant questions in predicting room air motion," ASHRAE Transactions, vol.98(1), pp.929–38, 1992.
[22] PG. Schild, PO. Tjelflaat, D. Aiulfi, "Guidelines for CFD modeling of atria," ASHRAE Transaction, vol.101(2), pp.1311–29, 1995.
[23] B.Kader, Temperature and concentration profiles in fully turbulent boundary layers," Int. J.Heat Mass Transfer vol.24, pp.1541-1544, 1993.
[24] M. Wolfstein, "The Velocity and Temperature Distribution of One-Dimensional Flow with Turbulence Augmentation and Pressure Gradient," Int. J. Heat Mass Transfer, vol.12, pp.301-318, 1969.